CONTENTS

LIST OF TABLES

LIST OF FIGURES

1

QUATERNION FUNDAMENTALS

ch:quat

Quaternions were developed by Hamilton in 1866 [1] as an means of representing rotations in three dimensions. They are based on Euler's rotation theorem, whereby any rotation can be represented as a rotation by a single angle about a single axis. The various quaternion operations discussed in this thesis are are summarized below, following the discussion in [2].

A quaternion $\mathbf{q}$ is composed of a scalar component q_0 and a vector component $\vec{q} = (q_1, q_2, q_3)$. The quaternion is in essence an extension of complex numbers into three dimensions, where the scalar component is real and the vector components are orthogonal imaginary quantities:

$$\mathbf{q} = (q_0, \vec{q}) = q_0 + q_1 i + q_2 j + q_3 k \tag{1.1}$$

The imaginary axes i, j, k satisfy the following conditions:

$$\begin{aligned} i^2 &= j^2 = k^2 = -1, \\ ij &= -ji = k, \\ jk &= -kj = i, \\ ki &= -ik = j. \end{aligned} \tag{1.2}$$

{eq:quat_cond}

The complex conjugate is then $\mathbf{q}^* = (q_0, -\vec{q})$. The conditions eq. (1.2) imply that multiplication of two quaternions is not commutative. Working through the complex arithmetic, the product of two quaternions $\mathbf{p}$ and $\mathbf{q}$ can be written as

$$\mathbf{pq} = (p_0 q_0 - \vec{p}\cdot\vec{q}, p_0\vec{q} + q_0\vec{p} + \vec{p}\times\vec{q}). \tag{1.3}$$

From eq. (1.3), we find that the quaternion norm is $|\mathbf{q}|^2 = \mathbf{q}^*\mathbf{q} = q_0^2 + |\vec{q}|^2$. The inverse of a quaternion, which satisfies $\mathbf{q}^{-1}\mathbf{q} = 1$, is $\mathbf{q}^{-1} = \mathbf{q}^*/|\mathbf{q}|^2$. A normalized (unit) quaternion, with $|\mathbf{q}| = 1$, provides a compact representation of a rotation about a unit axis $\vec{u}$ by an angle θ:

$$R_{\vec{u}}(\theta) = (\cos\frac{\theta}{2}, \sin\frac{\theta}{2}\vec{u}). \tag{1.4}$$

A sequence of rotations is then simply a multiplication of quaternions as in eq. (1.3). To apply a rotation $\mathbf{q}$ to an arbitrary vector $\vec{v}$, we treat the vector as a purely imaginary quaternion $\boldsymbol{v} = (0, \vec{v})$, and rotation is performed as a *conjugation* of $\boldsymbol{v}$ by $\mathbf{q}$:

$$\boldsymbol{v}' = \mathbf{q}\boldsymbol{v}\mathbf{q}^{-1}. \tag{1.5}$$

This is equivalent to multiplying $\vec{v}$ by the matrix

$$M(\mathbf{q}) = \begin{pmatrix} q_0^2 + q_1^2 - q_2^2 - q_3^2 & 2(q_1q_2 - q_0q_3) & 2(q_1q_3 + q_0q_2) \\ 2(q_1q_2 + q_0q_3) & q_0^2 - q_1^2 + q_2^2 - q_3^2 & 2(q_2q_3 - q_0q_1) \\ 2(q_1q_3 - q_0q_2) & 2(q_2q_3 + q_0q_1) & q_0^2 - q_1^2 - q_2^2 + q_3^2 \end{pmatrix}. \tag{1.6}$$

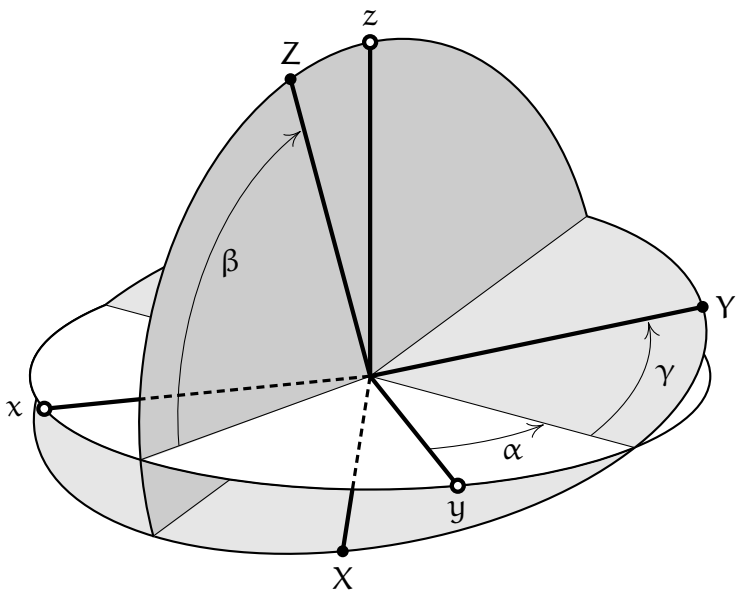

FIGURE 1.1: ZYZ Euler angles used throughout this thesis. Shown are the longitudinal and latitudinal angles (α, β) between the fixed (xyz) and rotated (XYZ) frames that define the direction of the Z-axis, and the rotation angle γ about the Z-axis. Note that here β is defined as the compliment of the angle between the fixed and rotated polar axes.

fig:euler_angles

Astronomical coordinates are typically defined in terms of the ZYZ-form Euler angles, as shown in Figure 1.1. The rotation matrix form for these angles is

$$R_Z(\alpha)R_Y\left(\tfrac{\pi}{2}-\beta\right)R_Z(\gamma) = \begin{pmatrix} c_\alpha s_\beta c_\gamma - s_\alpha s_\gamma & -s_\alpha c_\gamma - c_\alpha s_\beta s_\gamma & c_\alpha c_\beta \\ c_\alpha s_\gamma + s_\alpha s_\beta c_\gamma & c_\alpha c_\gamma - s_\alpha s_\beta s_\gamma & s_\alpha c_\beta \\ -c_\beta c_\gamma & c_\beta s_\gamma & s_\beta \end{pmatrix}, \quad (1.7)$$

{eq:euler_mat}

where (c_ϕ, s_ϕ) are shorthand for $(\cos\phi, \sin\phi)$. Comparing eq. (1.6) to eq. (1.7), we obtain expressions for the Euler angles in terms of the elements of the unit

quaternion. First, for the case when $\cos\beta \neq 0$, we use the elements of the third column and third row of the rotation matrix to obtain:

$$\begin{aligned} \alpha &= \operatorname{atan2}\left(q_2 q_3 - q_0 q_1,\ q_1 q_3 + q_0 q_2\right) \\ \sin\beta &= q_0^2 - q_1^2 - q_2^2 + q_3^2 \\ \sin 2\gamma &= 2\left(q_0 q_1 + q_2 q_3\right)\left(q_0 q_2 - q_1 q_3\right) / \cos^2\beta \\ \cos 2\gamma &= 2\left(q_0 q_2 - q_1 q_3\right)^2 / \cos^2\beta - 1, \end{aligned} \tag{1.8}$$

{eq:quat_coords}

where $\operatorname{atan2}(y, x)$ accounts for the signs of the numerator and denominator in computing $\tan^{-1}(y/x)$, and the β and γ terms are written in the form typically required for proper decomposition of the Stokes Q and U parameters on the sphere. Note that we assume $\cos\beta > 0$, so that β is restricted to the range $[-\frac{\pi}{2}, \frac{\pi}{2}]$. In the case when $\cos\beta = 0$, we fix $\alpha = 0$ and solve for γ using the remaining matrix elements. If $\sin\beta = 1$, then

$$\begin{aligned} \sin 2\gamma &= 4 q_0 q_3 \left(q_0^2 - q_3^2\right), \\ \cos 2\gamma &= 2\left(q_0^2 - q_3^2\right)^2 - 1; \end{aligned} \tag{1.9}$$

{eq:quat_coords2}

and if $\sin\beta = -1$, then

$$\begin{aligned} \sin 2\gamma &= 4 q_1 q_2 \left(q_2^2 - q_1^2\right), \\ \cos 2\gamma &= 2\left(q_2^2 - q_1^2\right)^2 - 1. \end{aligned} \tag{1.10}$$

{eq:quat_coords3}

2

CELESTIAL COORDINATE TRANSFORMATIONS

ch:pnt

Efficient computation has become a significant concern with the exponential growth of the amount of data acquired by present-day CMB experiments. Various computational methods have been developed to speed up processing of data, but a significant bottleneck remains with reading data from, and writing to, on-disk storage. One major concern is how to efficiently store and compute pointing data for each of thousands of individual channels.

A natural way to store pointing information is using a time-ordered set of horizon coordinates

- a azimuth,
- e elevation,
- p pitch,
- r roll,
- λ Earth longitude,
- ϕ Earth latitude, and
- t UTC time.

These indicate the orientation of the telescope boresight with respect to the Earth's horizon. Typically many channels are arranged in the telescope focal plane such that each channel is observing a slightly different location on the sky relative to the boresight direction. The orientation of each channel on the sky is a time-ordered set of celestial coordinates

α right ascension,
δ declination, and
φ position angle.

In order to determine the direction each individual channel is pointing at any given time, the boresight horizon coordinates must be rotated into the celestial frame, and shifted by the pre-determined pointing offset of each channel. The attitude of a single channel $\mathbf{q}_c$ in celestial coordinates can be expressed in terms of the boresight attitude in horizon coordinates using the following quaternion expression:

$$\mathbf{q}_c = A_a \left(\mathbf{q}_C(t)\ \mathbf{q}_T(t)\ A_d \left(F_r \left(\mathbf{q}_H(t)\ \mathbf{q}_\Delta\ \mathbf{q}_\psi(t)\right)\right)\right) \simeq \mathbf{q}_B(t)\ \mathbf{q}_\Delta\ \mathbf{q}_\psi(t). \tag{2.1}$$

{eq:pntalga}

Each of the terms in eq. (2.1) are discussed in more detail below.

The process of computing eq. (2.1) can be computationally intensive; therefore, the per-channel pointing solutions are often computed once and stored on disk. However, as the number of channels increases exponentially, reading such data from disk becomes prohibitively slow, so on-the-fly computation becomes necessary. The algorithm described in this text, based largely on the `libactpol` pointing library and the latest conventions of the International Earth Rotation and Reference Systems Service (IERS) [3], provides an efficient and parallelized method for calculating telescope pointing on the fly, with some control over the accuracy (and therefore, the speed) of the computation. The algorithm is implemented as part of the `qpoint` pointing library, which is used by the SPIDER team for pointing simulations as well as parallelized per-channel pointing computation and mapmaking in the analysis pipeline. We plan to release the `qpoint` code for public use by the astrophysics community.

2.1 CHANNEL OFFSET

The channel offset is expressed in terms of a beam centroid measured as a local azimuth Δa and elevation Δe relative to boresight $a = e = 0$, and angular orientation of polarization sensitivity ($\Delta\varphi$) as measured relative to the vertical. The offset quaternion $\mathbf{q}_\Delta$ is thus

$$\mathbf{q}_\Delta = R_x(-\Delta a)\, R_y(\Delta e)\, R_z(-\Delta\varphi), \tag{2.2}$$

{eq:quat_deltaa}

where the rotations $R_{\{x,y,z\}}$ are defined as in eq. (1.4). The channel offset is a stationary quantity throughout the observation period, and thus only needs to be computed once.

When a HWP is present in front of the bolometer, the position angle is offset by twice the waveplate angle ψ:

$$\mathbf{q}_\psi = R_z(-2\psi). \tag{2.3}$$

{eq:quat_delta_hwp}

In the case of a stepped HWP, it is most efficient to update the channel offset $\mathbf{q}_\Delta$ at each HWP step using eq. (2.3), rather than to treat the HWP angle as a separate time series.

2.2 ROTATION TO HORIZON FRAME

The offset quaternion $\mathbf{q}_\Delta$, defined in eq. (2.2), is rotated into the horizon frame by applying the quaternion $\mathbf{q}_H$, which is defined in terms of the the boresight azimuth, elevation, pitch and roll as

$$\mathbf{q}_H = R_x(-r)\, R_y(-p)\, R_z(-a)\, R_y(\tfrac{\pi}{2} - e)\, R_z(\pi). \tag{2.4}$$

The horizon coordinates are measured using a variety of onboard sensors and encoders, as discussed in ??.

2.3 ATMOSPHERIC REFRACTION

The effects of refraction through the Earth's atmosphere are negligible at float altitudes, but in principle the elevation should be corrected for this as

$$e' = e_0 - \delta_r, \tag{2.5}$$

where the correction term δ_r depends on the local weather conditions (pressure, humidity, altitude), the observation wavelength, and the uncorrected elevation e_0 of the observer $\mathbf{q}$, which is

$$e_0 = \sin^{-1}\left(\left(\mathbf{q}\hat{z}\mathbf{q}^{-1}\right)\cdot\hat{z}\right). \tag{2.6}$$

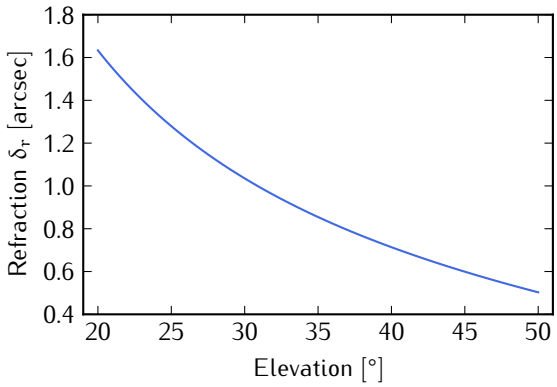

FIGURE 2.1: Refraction correction angle as a function of elevation, assuming 10 mbar atmospheric pressure and 0.1 % relative humidity at an altitude of 35 km.

fig:refraction

Writing the refraction correction in the form of a quaternion product, we have:

$$F_r(\mathbf{q}) = \mathbf{q}\ R_z(-\pi)\ R_y(\delta_r)\ R_z(\pi) = \mathbf{q}\ R_y(-\delta_r). \tag{2.7}$$

{eq:quat_ref}

The refraction correction is expected to be $<2''$ throughout SPIDER's elevation range, and vary over the 20° field of view by no more than $0.5''$, assuming 10 mbar atmospheric pressure and 0.1 % relative humidity at an altitude of 35 km. fig:refraction Figure 2.1 shows the correction δ_r as a function of elevation for these weather conditions.

2.4 DIURNAL ABERRATION

The aberration of light due to motion of the observer induces an apparent shift in the location of objects on the sky, as shown in fig:aberration Figure 2.2. The aberration correction depends on the orientation of the observer, thus cannot be applied as a simple rotation. For an observer $\mathbf{q}$ moving with velocity $\vec{\beta} = \vec{v}/c$ and looking along the

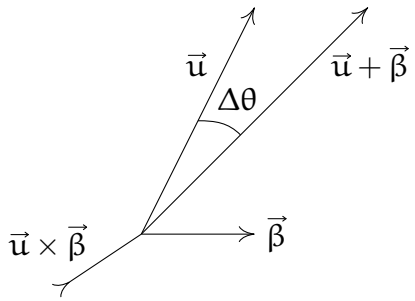

FIGURE 2.2: Aberration of light due to motion of the observer. The apparent direction $\vec{u}+\vec{\beta}$ is realized by rotating the geometric direction $\vec{u}$ about the normal $\vec{u}\times\vec{\beta}$ by an angle $\Delta\theta = \sin^{-1}|\vec{u}\times\vec{\beta}|$.

fig:aberration

direction $\vec{u} = \mathbf{q}\hat{z}\mathbf{q}^{-1}$ in the co-moving reference frame, the aberration correction is

$$\mathbf{q}' = A(\mathbf{q}) = R_{\hat{n}}(-\Delta\theta)\ \mathbf{q}, \tag{2.8}$$

{eq:quat_aber}

where the rotation is applied about the direction $\vec{n} = \vec{u}\times\vec{\beta}$, by the angle $\sin\Delta\theta = |\vec{n}|$.

The angular velocity of the Earth's surface at the equator is $|\vec{\beta}| \simeq 0.3''$, thus the diurnal aberration correction A_d for an Antarctic observer is typically $<0.1''$, which is negligible given SPIDER's pointing accuracy requirements. The correction can be ignored altogether, or applied solely at the boresight orientation to average the correction over the field of view. In the latter case, we apply the approximation

$$A(\mathbf{q}\ \mathbf{q}_\Delta) \simeq A(\mathbf{q})\,\mathbf{q}_\Delta = \mathbf{q}'\mathbf{q}_\Delta, \tag{2.9}$$

{eq:quat_aber_simple}

so that eq. (2.1) simplifies to

$$\mathbf{q}_c = A_a \left(\mathbf{q}_C \, \mathbf{q}_T \, \mathbf{q}'_H \, \mathbf{q}_\Delta \right). \tag{2.10}$$ {eq:pntalg2}

2.5 ROTATION TO TERRESTRIAL FRAME

The corrected horizon orientation is then rotated into a reference frame that is co-rotating with the Earth, using the latitude and longitude of the telescope:

$$\mathbf{q}_T = R_z(\lambda) \, R_y(\tfrac{\pi}{2} - \phi) \, R_z(\pi). \tag{2.11}$$ {eq:quat_ter}

These coordinates are provided by an onboard GPS every 30 seconds for SPIDER. For a ground-based instrument, these coordinates are of course fixed.

2.6 ROTATION TO CELESTIAL FRAME

Rotating the channel coordinates from the terrestrial frame onto the sky requires knowledge of the Earth's orientation relative to the barycentric celestial reference frame with high precision. Following the conventions in Chapter 5 of [3], the transformation is performed in three steps:

$$\mathbf{q}_C = \mathbf{q}_P \, \mathbf{q}_R \, \mathbf{q}_W \tag{2.12}$$ {eq:quat_cel}

where $\mathbf{q}_W$ accounts for the "wobble" of the Earth's rotation axis relative to the terrestrial reference frame; $\mathbf{q}_R$ accounts for the rotation of the terrestrial frame

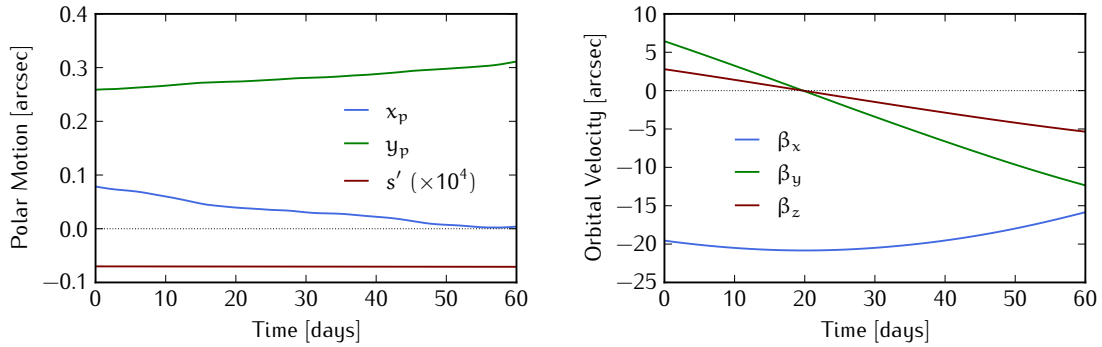

(a) Polar motion parameters throughout December 2014 and January 2015.

(b) The components of the Earth's orbital velocity during the same period.

FIGURE 2.3: Amplitudes of several correction terms discussed in the text.

relative to the celestial frame; and $\mathbf{q}_P$ accounts for the motion of the Earth's pole due to precession and nutation about the solar orbit. Various astronomical libraries [*e.g.*, 4] provide codes for calculating these terms, as summarized below.

The Earth's wobble is constructed as

$$\mathbf{q}_W = R_3(s')\, R_2(-x_p)\, R_1(-y_p), \tag{2.13}$$

where (x_p, y_p) are the coordinates of the pole in arcseconds, and s' is the displacement of the terrestrial meridian. The polar coordinates are tabulated daily in IERS Bulletin A [5]. These are typically no larger than $0.5''$ and vary on the timescale of a year, so are thus negligible for SPIDER's pointing requirements. In practice, $s' < 0.4\,\mathrm{mas}$ [3], and is thus entirely negligible for most cosmological purposes. Figure 2.3a shows the variation in the wobble parameters throughout the 2014/2015 austral summer.

The rotation of the Earth relative to the barycentric frame is calculated as a function of the sidereal angle ϵ as

$$\mathbf{q}_R = R_3(\epsilon). \tag{2.14}$$ {eq:quat_era}

Finally, precession and nutation of the Earth's orbit relative to the J2000 epoch is accounted for by

$$\mathbf{q}_P = R_3(E)\, R_2(d)\, R_3(-E - s), \tag{2.15}$$ {eq:quat_npb}

where the polar coordinates (E, d) are calculated from the vector coordinates (X, Y) as

$$E = \operatorname{atan2}(Y, X), \qquad d = \cos^{-1}\sqrt{1 - X^2 - Y^2}, \tag{2.16}$$ {eq:npb_coords}

and the parameter s describes the displacement of the celestial meridian. The parameters (X, Y, s) are calculated using the IAU 2006/2000A model for full accuracy, or the IAU 2000B model for more efficient computation at reduced accuracy. A comparison of the parameters calculated using these two models is shown in Figure 2.4. {fig:npb_comp} The 2000B model, which is twelve times more efficient than the 2006/2000A model[1], is more than adequate for SPIDER's purposes.

1 As measured on a Macbook Pro with a 2.5 GHz Core i5 processor and 8 GB RAM

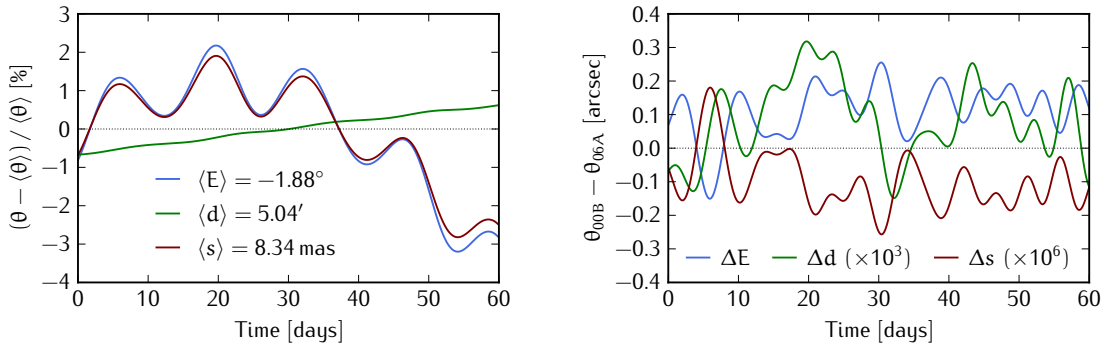

(a) Fractional variation of nutation/precession parameters throughout December 2014 and January 2015.

(b) Absolute difference between full and reduced nutation/precession models during the same period.

FIGURE 2.4: Comparison of the full 2006/2000A and reduced 2000B models for nutation and precession.

fig:npb_comp

2.7 ANNUAL ABERRATION

The final correction applied to recover the celestial coordinates of each channel is the stellar aberration correction due to the orbit of the Earth. The orbital velocity is calculated in the barycentric reference frame using pre-computed ephemerids [4], and the correction is applied according to eq. (2.8). The average velocity is approximately 20″ (Figure 2.3b). While this correction is small, it is comparable to the expected accuracy of the post-flight pointing reconstruction, so in principle it should be accounted for to ensure that the aberration correction is subdominant. As a compromise, a mean correction can be applied to all channels using the approximation eq. (2.9), so that eq. (2.10) reduces to

$$\mathbf{q}_c = \mathrm{A}_\alpha\left(\mathbf{q}_C\,\mathbf{q}_T\,\mathbf{q}'_H\,\mathbf{q}_\Delta\right) \simeq \mathrm{A}_\alpha\left(\mathbf{q}_B\right)\mathbf{q}_\Delta = \mathbf{q}'_B\mathbf{q}_\Delta, \tag{2.17}$$

{eq:pntalg3}

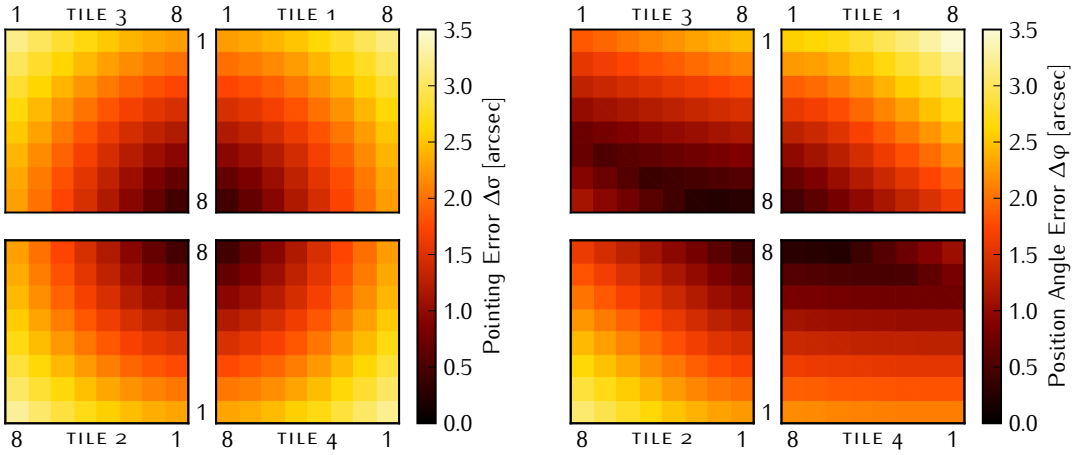

(a) The great circle distance $\Delta\sigma$ between the corrected and uncorrected celestial coordinates (α, β).

(b) The difference between the corrected and uncorrected position angle φ.

fig:pnt_err_pol

fig:pnt_err_sigma

FIGURE 2.5: Maximum error in reconstructed channel pointing if the effect of annual aberration relative to the boresight orientation is left uncorrected. The error is calculated using a simulated pointing dataset computed over one sidereal day, using a complete SPIDER 150 GHz focal plane of 512 polarized channels clocked at 22.5° about the boresight.

fig:pnt_err

where the second equality defines the pointing quaternion $\mathbf{q}_B$ for the boresight direction.

The annual aberration correction varies by as much as several arcseconds across the focal plane throughout the sidereal day, as shown in Figure 2.5. While the amplitude is small, the error has a coherent shape across the focal plane, which could induce a systematic signal in the data. Signal simulations, performed using the pipeline outlined in **??**, can be used to show whether ignoring this pointing error for the sake of efficiency would induce a significant systematic effect.

It is important to note that any measurement of the CMB temperature is also aberrated by the motion of the observer [6]. However, this correction can be ap-

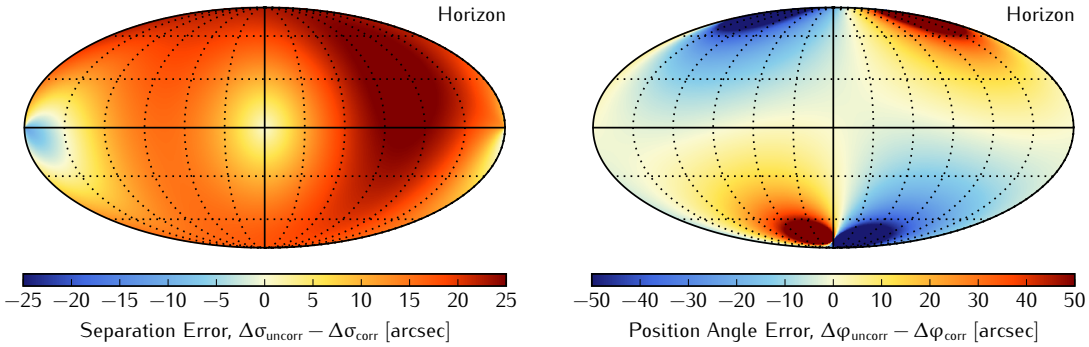

(a) The difference between the corrected and uncorrected great circle separation $\Delta\sigma$ between star cameras.

(b) The difference between the corrected and uncorrected relative position angle $\Delta\varphi$ between star cameras.

fig:sc_err_sigma fig:sc_err_pol

FIGURE 2.6: Error in the angular separation of a pair of star cameras, as determined from their respective celestial pointing solutions, if the effect of annual aberration is not taken into account. The error is shown as a function of the horizon coordinates of one star camera, assuming the second camera is fixed at $a = e = 0$.

fig:sc_aber

plied in the map domain after the relative effects of aberration have been corrected in the pointing solution.

2.7.1 *Aberration of Star Camera Solutions*

sec:sc_aber

In practice, the SPIDER boresight pointing solution is computed from the orientation of the three star cameras observing the sky as the instrument scans in azimuth and elevation. Each star camera image is resolved to a celestial orientation using the true (deaberrated) star positions. Solutions from each of the star cameras are then combined with the gyroscope and elevation data to compute a boresight pointing solution at the bolometer data rate. However, because each star camera is pointing in vastly different directions on the sky relative to the other cameras, the *physical* orientation of each camera relative to the others, as computed from the

celestial pointing solutions, is modulated by the *relative* effect of aberration along each camera direction. The amplitude of this relative aberration effect is illustrated in fig:sc_aber Figure 2.6.

Correcting for aberration in the computation of the final boresight pointing solution thus requires computing the relative orientations of the star cameras in the *aberrated* celestial frame, in which the orientations of the cameras relative to each other are constant to first order (ignoring mechanical stresses due to motion of the gondola). A more accurate boresight solution should thus be computed using the following procedure:

1. Aberrate each star camera solution using the inverse of eq:quat_aber eq. (2.8).
2. Compute the boresight pointing solution in the aberrated reference frame.
3. De-aberrate the final boresight pointing solution using eq:quat_aber eq. (2.8).

This algorithm should reduce errors due to modulation of the star camera orientation on the sky as the cameras move relative to each other and relative to the Earth's velocity throughout the day.

2.8 ALGORITHM IMPLEMENTATION

sec:qpoint

The pointing algorithm is implemented in a way that allows control over the accuracy (and therefore, the efficiency) of the calculations described in the previous section. The procedure is divided into steps, as shown in tab:pnt_tune Table 2.1. For steps involving small correction terms, such as the aberration and polar motion corrections, the user can control the sample rate at which the relevant quaternions are updated. Because the pointing data are processed in a time-ordered way, correction

terms can be updated every N^{th} sample to speed up processing without significant loss of accuracy. This is especially useful for computationally intensive corrections like the celestial polar motion quaternion $\mathbf{q}_P$, which involves hundreds of linear operations to compute, yet varies slowly enough that it can be updated rarely. Additionally, the refraction and aberration corrections can be applied to the boresight quaternion $\mathbf{q}_B$ once as in eq. (2.9), effectively averaging the correction across the focal plane. Finally, some correction terms are small enough that they can simply be ignored altogether for most cosmological applications; these are included in the software library for completeness.

tab:pnt_tune

TABLE 2.1: Each step of the `qpoint` algorithm for computing a single channel's orientation from boresight attitude to celestial coordinates. The third and fourth columns summarize the amount of control the user has over the computation at each step. Each correction or rotation can be applied once in the computation of $\mathbf{q}_B$ (as an effective average over the focal plane), or at each channel individually. Moreover, some correction terms which vary slowly enough are updated at a tunable sample rate. The sample rates selected for sufficiently accurate simulations of SPIDER pointing are indicated in the final column.

STEP	ADD'L INPUTS	FPU AVG?	TUNE RATE?	SAMPLE RATE[a]
$\mathbf{q}_\Delta$	$\Delta a, \Delta e, \Delta\varphi$	N	N	once
$\mathbf{q}_H$	a, e, p, r	Y	N	1
F_r	δ_r	Y[b]	Y	never
A_d	$\vec{\beta}_{rot}$	Y[b]	Y[d]	1
$\mathbf{q}_T$	λ, ϕ	Y	Y	1
$\mathbf{q}_W$	x_p, y_p, s'	Y	Y	never
$\mathbf{q}_R$	ϵ	Y	Y	1
$\mathbf{q}_P$	X, Y, s	Y	Y	10
A_a	$\vec{\beta}_{orb}$	Y[c]	Y[d]	100
α, β, φ	ψ[e]	N	N	1

[a] Corrections are calculated once and kept constant, never calculated at all, or calculated at the indicated rate of samples between updates.
[b] The focal-plane-averaged correction is applied by default. Correcting each channel individually requires repeating all subsequent steps.
[c] The correction is applied to each channel by default, but the user can choose to apply a focal-plane averaged correction instead.
[d] The rate at which the velocity vector $\vec{\beta}$ is updated is commandable, but the rotation is calculated as in eq. (2.8) and applied at the sample rate.
[e] The HWP angle ψ can optionally be applied as an independent correction rather than a term included in the position angle offset $\Delta\varphi$.

BIBLIOGRAPHY

hamilton1866 [1] W. R. Hamilton. *Elements of Quaternions*. London, Longmans, Green & Co., 1866.

kovalevsky2004 [2] J. Kovalevsky and P. K. Seidelmann. *Fundamentals of Astrometry*. Cambridge University Press, Cambridge, UK, June 2004.

iers2010 [3] G. Petit and B. Luzum. IERS conventions. IERS Technical Note 36, Frankfurt am Main: Verlag des Bundesamts für Kartographie und Geodäsie, 2010.

sofa [4] IAU SOFA Board. Iau sofa software collection. URL: http://www.iausofa.org.

iers_bulla [5] Earth Orientation Department of the U.S Naval Observatory. Iers rapid service prediction center for earth orientation parameters. URL: http://maia.usno.navy.mil.

planck_aber [6] Planck Collaboration, N. Aghanim, C. Armitage-Caplan, M. Arnaud, M. Ashdown, F. Atrio-Barandela, J. Aumont, C. Baccigalupi, A. J. Banday, R. B. Barreiro, J. G. Bartlett, K. Benabed, A. Benoit-Lévy, J.-P. Bernard, M. Bersanelli, P. Bielewicz, J. Bobin, J. J. Bock, J. R. Bond, J. Borrill, F. R. Bouchet, M. Bridges, C. Burigana, R. C. Butler, J.-F. Cardoso, A. Catalano, A. Challinor, A. Chamballu, H. C. Chiang, L.-Y. Chiang, P. R. Christensen, D. L. Clements, L. P. L. Colombo, F. Couchot, B. P. Crill, A. Curto, F. Cuttaia, L. Danese, R. D. Davies, R. J. Davis, P. de Bernardis, A. de Rosa, G. de Zotti, J. Delabrouille, J. M. Diego, S. Donzelli, O. Doré, X. Dupac, G. Efstathiou, T. A. Enßlin, H. K. Eriksen, F. Finelli, O. Forni, M. Frailis, E. Franceschi, S. Galeotta, K. Ganga, M. Giard, G. Giardino, J. González-Nuevo, K. M. Górski, S. Gratton, A. Gregorio, A. Gruppuso, F. K. Hansen, D. Hanson, D. L. Harrison, G. Helou, S. R. Hildebrandt, E. Hivon, M. Hobson, W. A. Holmes, W. Hovest, K. M. Huffenberger, W. C. Jones, M. Juvela, E. Keihänen, R. Keskitalo, T. S. Kisner, J. Knoche, L. Knox, M. Kunz, H. Kurki-Suonio, A. Lähteenmäki, J.-M. Lamarre, A. Lasenby, R. J. Laureijs, C. R. Lawrence, R. Leonardi, A. Lewis, M. Liguori, P. B. Lilje, M. Linden-Vørnle, M. López-Caniego, P. M. Lubin, J. F. Macías-Pérez, N. Mandolesi, M. Maris, D. J. Marshall, P. G. Martin, E. Martínez-González, S. Masi, M. Massardi, S. Matarrese, P. Mazzotta, P. R. Meinhold, A. Melchiorri, L. Mendes, M. Migliaccio, S. Mitra, A. Moneti, L. Montier, G. Morgante, D. Mortlock, A. Moss, D. Munshi, P. Naselsky, F. Nati, P. Natoli, H. U. Nørgaard-Nielsen, F. Noviello, D. Novikov, I. Novikov, S. Osborne, C. A. Oxborrow, L. Pagano, F. Pajot, D. Paoletti, F. Pasian, G. Patanchon, O. Perdereau,

F. Perrotta, F. Piacentini, E. Pierpaoli, D. Pietrobon, S. Plaszczynski, E. Pointecouteau, G. Polenta, N. Ponthieu, L. Popa, G. W. Pratt, G. Prézeau, J.-L. Puget, J. P. Rachen, W. T. Reach, M. Reinecke, S. Ricciardi, T. Riller, I. Ristorcelli, G. Rocha, C. Rosset, J. A. Rubiño-Martín, B. Rusholme, D. Santos, G. Savini, D. Scott, M. D. Seiffert, E. P. S. Shellard, L. D. Spencer, R. Sunyaev, F. Sureau, A.-S. Suur-Uski, J.-F. Sygnet, J. A. Tauber, D. Tavagnacco, L. Terenzi, L. Toffolatti, M. Tomasi, M. Tristram, M. Tucci, M. Türler, L. Valenziano, J. Valiviita, B. Van Tent, P. Vielva, F. Villa, N. Vittorio, L. A. Wade, B. D. Wandelt, M. White, D. Yvon, A. Zacchei, J. P. Zibin, and A. Zonca. Planck 2013 results. XXVII. Doppler boosting of the CMB: Eppur si muove. A&A, 571:A27, November 2014. arXiv:1303.5087, doi:10.1051/0004-6361/201321556.